Modelling the Climate of the Eemian in Europe Using an Interactive Physical Downscaling

Frank Arthur *, Anhelina Zapolska, Didier M. Roche, Huan Li, Hans Renssen

Posted Date: 5 February 2025

doi: 10.20944/preprints202502.0262.v1

Keywords: The Eemian; The Holocene; Europe; iLOVECLIM; Interactive Downscaling; Climate modelling; The Quaternary

 doi:10.20944/preprints202502.0262.v1

Article

Modelling the Climate of the Eemian in Europe Using an Interactive Physical Downscaling

Frank Arthur [1], Anhelina Zapolska [2], Didier M. Roche [2,3], Huan Li [4] and Hans Renssen [1]

[1] Department of Natural Sciences and Environmental Health, University of South-Eastern Norway, Bø, Norway
[2] Earth and Climate Cluster, Faculty of Science, Vrije Universiteit Amsterdam, Amsterdam, the Netherlands
[3] Laboratoire des Sciences du Climat et de l'Environnement, LSCE/IPSL, CEA-CNRS-UVSQ, Université Paris-Saclay, Gif-sur-Yvette, France
[4] School of Geographic Science, Nantong University, Nantong 226019, China
* Corresponding Frank.Arthur@usn.no and Hans.Renssen@usn.no

Abstract: The Eemian interglacial (~130 - 116 ka) is a period characterized by a significantly warmer climate than the pre-industrial era, providing a valuable opportunity to study natural climate variability and its implications for the future. We studied the Eemian climate in Europe by applying an interactive downscaling to our Earth system model (iLOVECLIM) to increase its horizontal atmospheric resolution from 5.56° to 0.25° latitude-longitude. A transient simulation was conducted for both the standard version of the model and with an interactive downscaling applied for the Eemian (127 – 116 ka). Our simulations suggest that the magnitude of temperature and precipitation varied across different regions of Europe, with some areas experiencing more pronounced warming and precipitation changes than others. The latitudinal pattern in our simulation during the Eemian shows that the warming in Europe was stronger at high latitudes than at mid-latitudes. Relative to the pre-industrial climate, our downscaling scheme simulates at 127 ka higher temperatures between 3 – 4 °C in the northern part of Europe and higher precipitation values between 150 – 300 mm/yr. Our results indicate that, in comparison to the standard model, the downscaled simulations offer spatial variability that is more in line with proxy-based reconstructions and other climate models.

Keywords: The Eemian 2; The Holocene 3; Europe 4; iLOVECLIM 5; Interactive Downscaling 6; Climate modelling 7; The Quaternary

1. Introduction

The Quaternary era is known for its distinct changes between long relatively cold glacial periods and shorter interglacial periods with a warmer climate, like the current Holocene era (Brewer et al., 2008). The previous warm period called the Last Interglacial, or Eemian (~130–116 ka), had global mean temperatures of about 2 °C warmer than the pre-industrial (Turney and Jones, 2010). Some regions in the Northern Hemisphere were even up to 5 °C warmer than the mean of the last millennium (NEEM, 2013), and global sea levels were up to 5 m higher than present day, reflecting smaller ice sheets (Dutton and Lambeck, 2012; Dyer et al., 2021). Paleoclimate simulations and reconstructions of this interglacial period are important because they serve as the most recent comparison for the present interglacial period, and because of the negligible impact of humans during the Eemian (Brewer et al., 2008; Otto-Bliesner et al., 2017). Moreover, the magnitude of the global temperature and sea surface temperature differences determined for the Eemian are comparable to the projected future climate in the second half of the 21st century (Otto-Bliesner et al., 2017). Therefore, studying the Eemian climate will provide information that can be useful in improving our understanding of future climate change and developing strategies to mitigate its impacts. This makes the study of the climate's evolution and sensitivity throughout an interglacial

 doi:10.20944/preprints202502.0262.v1

period and during a period when there was no human impact very important (Cheddadi et al., 1998). Another significant aspect of the Eemian climate that makes it valuable to study are the different forcings contributing to the warming compared to pre-industrial, which include orbital fluctuations during the Eemian. Compared to the Holocene, the Eemian was characterized by stronger insolation changes (Berger, 1978) but had relatively similar greenhouse gas (GHG) concentrations.

The availability of good proxy-based reconstruction data provides the opportunity to identify weaknesses in the model that could potentially be improved, resulting in more accurate projections of future climate (Braconnot et al., 2012; Otto-Bliesner et al., 2013; Otto-Bliesner et al., 2017). Several paleoclimate studies have been made to investigate the Eemian. Examples are available for climate model simulations (Fischer and Jungclaus, 2010; Bakker et al., 2014; Lunt et al., 2013; Goelzer et al., 2016; Pedersen et al., 2017; Li et al., 2020; Otto-Bliesner et al., 2021) and proxy-based climate reconstructions (Klotz et al., 2003; CAPE Last Interglacial Project Members, 2006; Brewer et al., 2008; Turney and Jones, 2010; McKay et al., 2011). These studies suggest that the warmest and wettest conditions in Europe occurred early in the Eemian (127 ka), followed by a steady decline in temperatures and precipitation.

The Eemian vegetation in some parts of Europe, such as the Alps, has been studied extensively by Klotz et al. (2004), with pollen records from a wide distribution of sites. In general, their reconstructions suggest that the forests in Europe were more extensive relative to pre-industrial, covering much of central and northern Europe. The pollen-based reconstruction of Klotz et al. (2004) also suggests that there was a greater abundance of deciduous trees than present day, such as birch which was later replaced by oak forest.

Although there have been a lot of climate modelling studies focusing on the Eemian, most of these studies employ General Circulation Models (GCMs), which have a coarse spatial resolution that implies a mismatch in spatial scale relative to proxy-based reconstructions, making comparisons with proxy data quite problematic. In this study, we performed transient simulations with both the standard version of the iLOVECLIM model (Roche et al., 2014) and a version in which downscaling was applied (Quiquet et al., 2018). This study provides detailed information on the Eemian climate by using a physical interactive downscaling in iLOVECLIM by Quiquet et al. (2018), to increase the resolution of the model from 5.56° to 0.25° latitude-longitude. The results were then compared to the low-resolution version of the model and proxy data to evaluate the impact of downscaling on the model. In addition, we compared our simulated Eemian climate with results from a similar downscaling experiment performed for the Holocene (Arthur et al., 2023). Thus, the research questions below are addressed in this study.

1. *What are the magnitudes and spatial patterns of temperature and precipitation changes over Europe during the Eemian period?*

2. *How do the simulated changes in temperature and precipitation compare to proxy data from the Eemian period? Is the downscaling performing better than the low-resolution model?*

3. *How different are the evolutions of the European climate in the Holocene and the Eemian?*

2. Materials and Methods

2.1. Model Description

2.1.1. The iLOVECLIM Model

As a climate model, we used iLOVECLIM version 1.0 (Roche et al., 2014), a code fork of LOVECLIM 1.2 (Goosse et al., 2010). The version of iLOVECLIM applied in this study is an Earth System Model of Intermediate Complexity with three main components: an atmosphere component (ECBILT), an ocean component (CLIO) and a vegetation component (VECODE). ECBilt is a quasi-geostrophic atmospheric model comprised of three vertical layers at T21 horizontal resolution (~5.625° × ~5.625° latitude–longitude) (Opsteegh et al., 1998). CLIO is an oceanic General Circulation Model with 20 unevenly spaced vertical layers at a 3◦ × 3◦ latitude–longitude horizontal resolution

 doi:10.20944/preprints202502.0262.v1

(Goosse and Fichefet, 1999). VECODE is a simplified dynamic global vegetation model (DGVM), that uses two plant functional types (PFTs), trees and grass, and bare ground as a third dummy type, with their fraction always amounting to 100% in the ECBILT grid cell (Brovkin et al., 1997). Several simulations such as the Holocene (Renssen et al., 2009; Zhang et al., 2018, Li et al., 2019; Arthur et al., 2023), LGM (Lhardy et al., 2021), last deglaciation (Quiquet et al., 2021), and last interglacial (Li et al., 2020) have been successfully conducted using iLOVECLIM.

Similar to Arthur et al. (2023), an interactive downscaling has been applied to the iLOVECLIM model in this study, to increase its spatial resolution in Europe from 5.56° to 0.25° latitude-longitude in Europe. The downscaling is performed on the original T21 grid. The fundamental approach of the downscaling is to explicitly consider the sub-grid orography by reproducing the model physics of ECBilt at a higher spatial resolution, rather than the dynamics. To do this, we create artificial vertical layers in the sub-grid orography, which allow us to compute variables like temperature and precipitation formation at any altitude. Quiquet et al. (2018) originally described the online interactive downscaling method integrated into iLOVECLIM and the physics used in the model is well explained in detail in their study (Quiquet et al., 2018). The downscaling method has been used previously to successfully simulate the transient Holocene climate in Europe by Arthur et al. (2023, 2024). These simulation results with downscaling for the Holocene suggest that temperature and precipitation are in better agreement with proxy data and other climate models in some European regions as compared to the standard version of the model.

2.1.2. Experimental Set-up

The results of two separate Eemian experiments were used in this study. The first experiment is a transient simulation of the Eemian (from 127 ka – 116 ka) performed by Li et al. (2020) using the low-resolution version of the iLOVECLIM 1.0 that includes the VECODE dynamic vegetation model (hereafter, EEM_Standard). The second experiment is also a transient simulation of the Eemian climate, but this time with the interactive downscaling applied to iLOVECLIM (Quiquet et al., 2018) to increase the resolution of the model (hereafter EEM_Down), identical to the technique used by Arthur et al. (2023). Both experiments were performed starting from an equilibrium experiment that was run for 3000 years with fixed forcings for 128 ka. The orbital forcings and greenhouse gas concentrations of CO_2, CH_4, and N_2O used in the transient simulations were the same as those used in the PMIP4 protocol (Otto-Bliesner et al., 2017). During a large part of the Eemian (approximately 127 – 119 ka), the NH received more insolation during the summer in June relative to pre-industrial values. (Figure 1). ILOVECLIM computes changes in the insolation received by the Earth during transient simulations based on astronomical parameters from Berger (1978). The CO_2 concentration fluctuated between 270 ppm and 280 ppm. However, CH_4 concentrations peaked at 127 ka (approximately 730 ppb) before declining steadily until the late Eemian (Figure 1). In addition to these Eemian experiments, we also compared our results with a downscaled transient simulation (hereafter HOL_Down) of the Holocene climate with the same resolution as the downscaled Eemian run published by Arthur et al. (2023).

We can assess different types of information from our results by evaluating the differences between our experiments. The difference between EEM_Down and EEM_ Standard provides information on the impact of the downscaling on our transient results for the Eemian. Finally, the difference between the Eemian and Holocene transient experiments provides information on how the European climate responds to the difference in forcing for the two interglacials.

 doi:10.20944/preprints202502.0262.v1

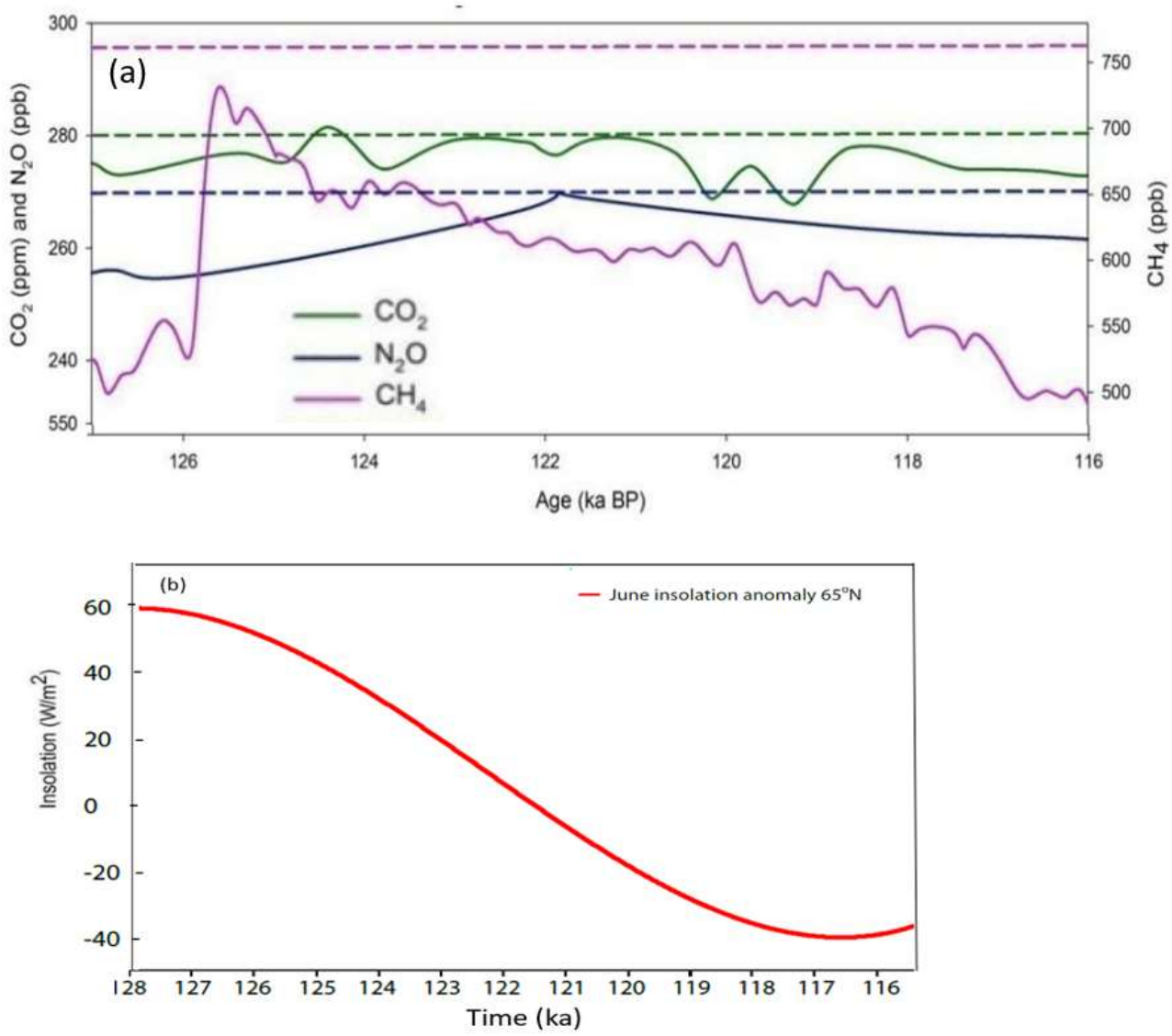

Figure 1. (a) from (Li et al., 2020). The climate forcings used for the simulations for EEM_Standard and EEM_Down (127 ka -116 ka). The greenhouse gas (GHG) concentrations of CO_2, CH_4, and N_2O are from the PMIP4 protocol (e.g., Schilt et al., 2010; Bereiter et al., 2015). The dashed lines represent the pre-industrial values. Figure 1 (b) shows the orbitally-forced June insolation for 65°N, provided as an anomaly from present-day values (Berger, 1978). .

3. Results and Discussion

3.1. The Spatial Distribution Of Annual Precipitation and Temperature Anomalies in Europe for the Eemian

Depending on the location of Europe, a comparison of the simulated annual mean temperature and precipitation anomalies relative to pre-industrial by both EEM_Down and EEM_Standard reveals several noteworthy similarities and variations in terms of magnitude and patterns of change. In general, both simulations show how much warmer it was during the Eemian. The EEM_Down, as predicted, offers more spatial variability and detailed information than the EEM_standard. The high-resolution grid shows the local temperature changes caused by the downscaling simulation.

3.1.1. Temperature

The EEM_Standard and the EEM_Down both agree on a clear north-south temperature gradient in Europe during the Eemian. The most significant temperature increase compared to the

 doi:10.20944/preprints202502.0262.v1

pre-industrial era was observed in Northernmost Europe, reaching up to +3°C at 127 ka (Figure 2). In contrast, Southern Europe experienced smaller temperature differences, with some areas even slightly cooler than the pre-industrial era. Later in the Eemie, the temperature gradient became less obvious, indicating the orbitally induced change in summer insolation (Figure 1b, Figure 2). When comparing the two model versions, the temperature gradient was more pronounced in EEM_Down, with warmer conditions in western Europe and northern Scandinavia than in EEM_Standard, particularly at 127 ka and 124 ka (Figure 2). The southeastern region of the domain and the Middle East, on the other hand, is cooler in EEM_Down than in EEM_Standard throughout the Eemian, with temperatures dropping to -2°C in comparison to the pre-industrial era.

Our model results, especially EEM_Down, show apparent, opposite latitudinal climate trends, including warming seen in the northernmost Scandinavia while cooling occurred in southeast Europe. This is likely due to the orbital forcings prescribed (mainly obliquity, i.e. changes in the Earth's axis tilt angle, and precession). This axial tilt angle was higher compared to pre-industrial in the early Eemian (~127 to 126 ka), resulting in more insolation at high latitudes and less insolation at low latitudes (Bakker et al., 2014). The June insolation anomaly at 127 ka for 65◦N was around 60 Wm^{-2}, relative to pre-industrial values (Berger, 1978). Another distinction is that during the early stages of the Eemian, perihelion occurred during summer in the Northern Hemisphere rather than during winter as it does today (i.e. the effect of precession, Bakker et al., 2014).

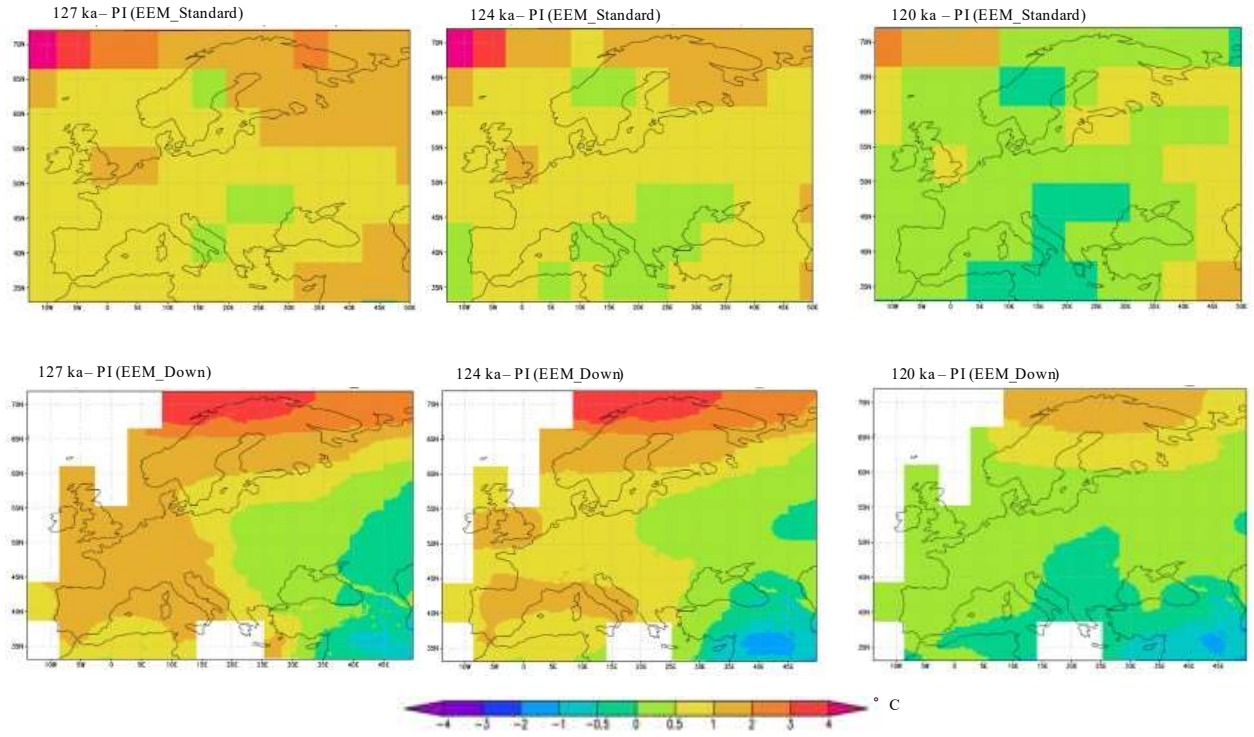

Figure 2. Mean annual temperature anomalies relative to pre-industrial mean simulated by the iLOVECLIM, showing spatial variability in Europe for 127 ka, 124 ka and 120 ka for EEM_Standard (top figures) and EEM_Down (bottom figures) in °C.

3.1.2. Precipitation

The results for precipitation from EEM_Standard, as illustrated in Figure 3, do not exhibit a pronounced spatial pattern, with fluctuations largely confined to the interval of -100 to +100 mm/yr. Conversely, EEM_Down presents a clear distribution, indicating some areas that are wetter than the pre-industrial, Relative to pre-industrial, there is a wet-dry-wet pattern that has a northwest-southeast direction, with the Atlantic coast (comprising Iberia, Ireland, Scotland, and the

 doi:10.20944/preprints202502.0262.v1

Scandinavian coast) being wetter, then succeeded by a drier zone that stretches from France and northern Italy to the northeast (Finland and Northern Russia), and finally, wetter conditions in the southeastern section of the domain. The dry region is interrupted by moderately wetter conditions found in central Europe. In the EEM_Down results, this wet-dry-wet pattern is most noticeable at 127 ka and becomes less pronounced in the late Eemian. The drier zone receives a decrease in precipitation of at least less than -200 mm/yr centered around the Alps, while the Atlantic coast and the southeast portion of the domain receive more than 300 mm/yr more precipitation than pre-industrial.

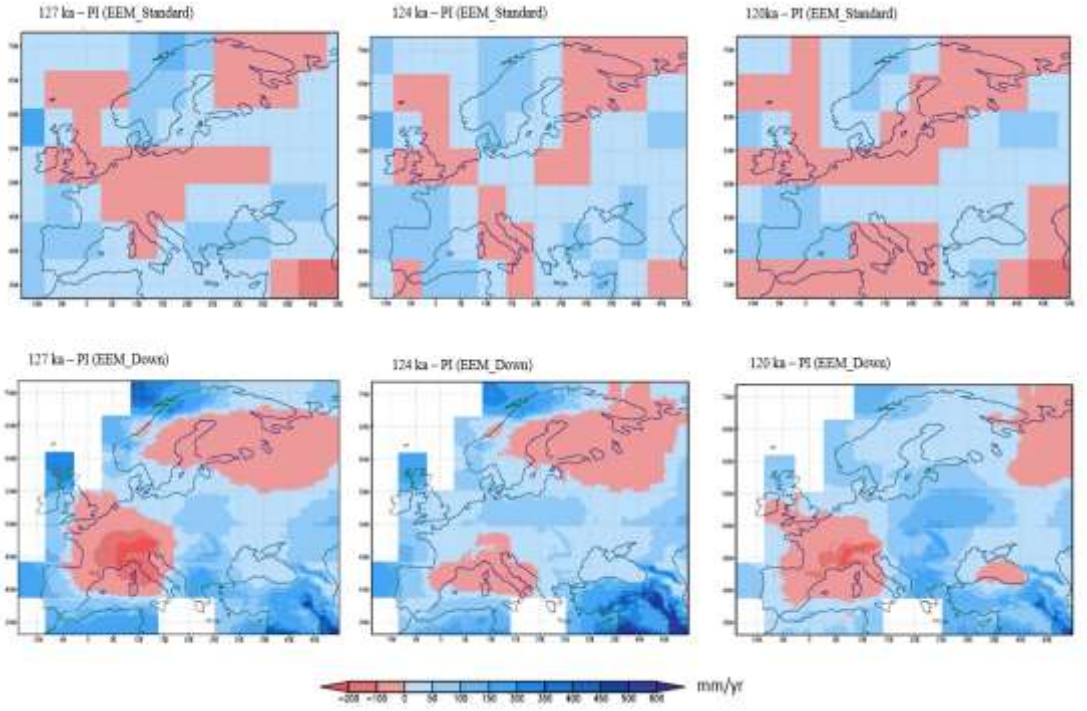

Figure 3. Mean annual precipitation anomalies relative to pre-industrial mean simulated by iLOVECLIM (in mm/yr), showing the spatial variability in Europe for 127 ka, 124 ka and 120 ka for EEM_Standard (top figures) and EEM_Down (bottom figures).

Downscaling increases precipitation in many elevated areas, like the Scottish Highlands and Scandes Mountains, leading to higher anomalies. Results with downscaling better reflect topography effects, with experiments showing wetter regions in Europe. In general, experiment EEM_Down is relatively wet compared to EEM_Standard in regions with complex topography.

3.2. The Evolution of Annual Temperature And Precipitation for the Eemian in Europe

The general temporal trends in temperature and precipitation in Europe display an overall cooling from the early to the late Eemian. Simulated temperature anomalies relative to pre-industrial indicate that at 127 ka, temperatures were 2.5 °C warmer than pre-industrial for EEM_Standard and 2 °C warmer in EEM_Down and started declining steadily after 126 ka in both simulations (Figure 4). A gradually decreasing trend with the warmest conditions in the first part of the experiments is thus observed. Temperatures started decreasing in the mid-Eemian with mean anomalies between (1 – 1.5 °C) around 123 ka for EEM_Down and 2 °C for EEM_Standard. The general decline continues further till 117 ka. EEM_Standard was generally warmer than EEM_Down,

 doi:10.20944/preprints202502.0262.v1

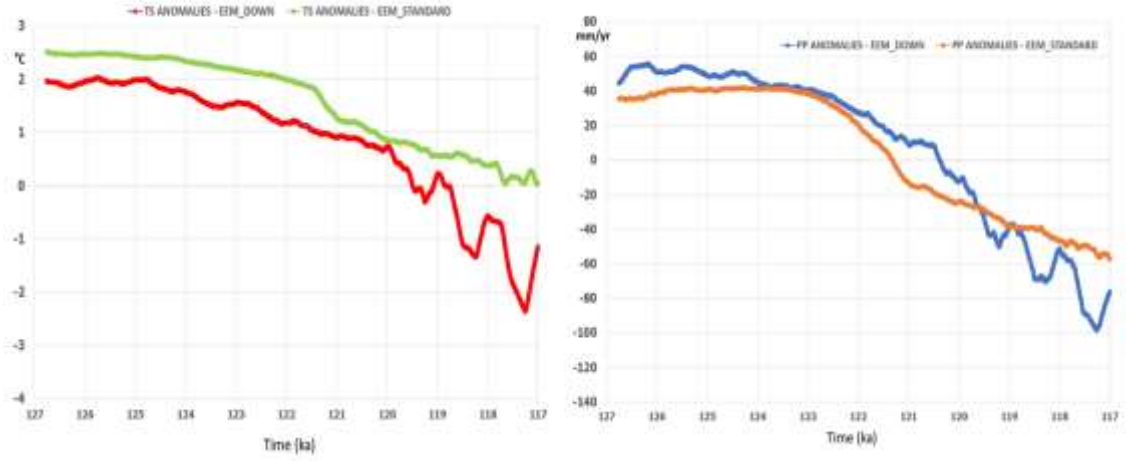

Figure 4. The annual temporal evolution of temperature (Left in °C) and precipitation (Right, in mm/yr) anomalies relative to pre-industrial in Europe with EEM_standard and EEM_Down. Light green colour: (Temperature, EEM_Standard), Red colour: (Temperature, EEM_Down), Orange colour: (Precipitation, EEM_Standard) and Blue colour: (Precipitation, EEM_Down). The trends show a 500-yr running mean.

The precipitation in EEM_Down was generally higher than EEM_Standard until after 119.5 ka as expected due to the impact of the downscaling. The annual average precipitation in Europe for the whole Eemian was 630.5 mm/yr and 623.5 mm/yr for EEM_down and EEM_Standard, respectively. Generally, the early and mid-Eemian were wetter than the late Eemian in both simulations, especially between 127 and 123 ka (Figure 4). For the EEM_Down and EEM_Standard experiments, precipitation was higher at 127 ka than pre-industrial with annual anomalies of 45 mm/yr and 35 mm/yr respectively, and both started rising again exceeding annual precipitation anomalies of 50 mm/yr (EEM_Down) and 40 mm/yr (EEM_Standard) relative to pre-industrial before steadily declining after 124 ka (Figure 4). There was a rapid decrease in precipitation after 123 ka to the late Eemian (Figure 4). The EEM_Down simulations were still wetter than pre-industrial until at 121 ka when it started getting drier while the dryness started earlier after 122 ka for EEM_Standard.

3.3. Comparison Between the Eemian and Holocene climate in Europe

There are several similarities between the Eemian and the Holocene, as our results in Europe indicate that both periods have temperatures and precipitation that were higher than the pre-industrial in the early stages and declined steadily to the pre-industrial level (Figure 5). However, the Eemian was warmer than the Holocene between 11 ka to 2.3 ka until after 119 ka for the Eemian (Figure 5). The Holocene and the Eemian climates are simulated with the same iLOVECLIM model, which offers the opportunity to analyze the impact of the forcings on the results. It has been found previously by Bakker et al. (2014) that both the Holocene and the Eemian are distinguished by significant changes in the temporal distribution of insolation, with many similarities. However, there are larger eccentricity values, a different regulation of obliquity and larger changes in precession during the Eemian compared to the Holocene, thus the magnitude of the annual, seasonal, and latitudinal insolation changes is larger during the Eemian than in the Holocene (Bakker et al., 2014). The melting of remnant ice sheets in the Holocene and potential ice sheet melt and expansion at the end of the Eemian period may have also affected the temperatures through feedbacks from ice sheet-ocean-circulation (Bakker et al., 2014). However, in our experiments the ice sheets were kept fixed at their present-day configurations, meaning that we were not able to account for these feedbacks.

 doi:10.20944/preprints202502.0262.v1

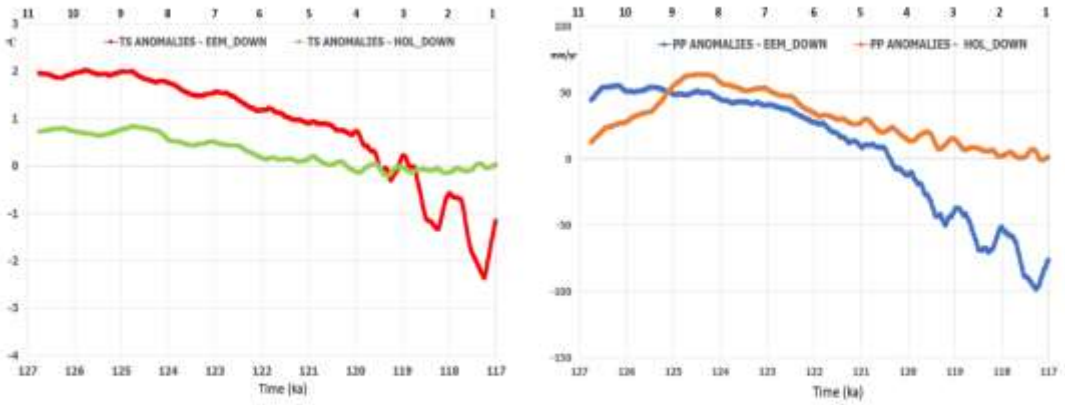

Figure 5. Showing annual mean temperature (left) and precipitation (right) anomalies relative to pre-industrial for the Holocene and the Eemian in Europe. Light green color: (Temperature, Holocene), Red colour: (Temperature, Eemian), Orange colour: (Precipitation, Holocene) and Blue colour: (Precipitation, Eemian). The trends show a 500-yr running mean.

For precipitation, the Eemian was about 40 mm/yr wetter in the early stages than the Holocene until after 9 ka when the Holocene became slightly wetter than the Eemian (Figure 5). Both the Holocene and the Eemian however, show a decreasing trend to the pre-industrial levels. The summer insolation at 65 ° N likely played a role in the declining trend of precipitation in both interglacials. The gradual decrease in precipitation was in response to the reduction in the summer insolation in both the Holocene and the Eemian epochs, forcing a decrease in temperature over time. Generally, a warmer atmosphere can hold more water vapour, leading to more precipitation. The higher precipitation anomalies recorded in the early Eemian compared to the early Holocene were probably due to the orbital forcings which were stronger during the early Eemian as compared to the early Holocene. It was however slightly wetter during the Holocene after 9 ka than the Eemian. The Holocene simulations done by Arthur et al. (2023) indicate that northernmost Europe was warmer at 9 ka than at 124 ka and this seems to correlate with the higher precipitation anomalies observed along the coast (Ireland, Scotland, and Norway) at 9 ka. The spatial pattern with relatively high temperatures in northernmost Europe is very similar to the pattern simulated for the early Holocene by Renssen et al. (2005). Renssen et al. (2005) showed that these warm conditions were reflecting a relatively strong Atlantic meridional overturning circulation (AMOC), combined with enhanced deep-water formation and reduced sea-ice cover in the Nordic Seas. The AMOC in the Nordic Seas and reduced sea-ice cover contributed to the redistribution of heat and moisture, influencing regional temperature patterns. In the Nordic Seas, warm, saline waters from the Atlantic Ocean flow northward, releasing heat and moisture into the atmosphere as they interact with cooler and fresher waters (Renssen et al., 2005). In the early Holocene up to 7 ka, the overturning in the Nordic seas is up to 10% than in the corresponding period in the Eemian (Figure 6). This is consistent with a simulated ~1° warmer surface of the North Atlantic Ocean in the early Holocene. A warmer Northernmost Europe at 9 ka is thus most likely related to a stronger AMOC than at 124 ka, providing relatively warm and moist air that favors precipitation in coastal areas. However, the differences in precipitation between 9 ka and 124 ka are relatively small and only become more expressed later in the interglacials (after 120 ka/ 4 ka) when the Eemian temperature becomes lower than the Holocene value (Fig 5), due to the increasing difference in orbital forcing.

 doi:10.20944/preprints202502.0262.v1

There is limited impact of the Arctic sea-ice cover on the temperature and precipitation patterns during the Holocene and the Eemian, as the simulations show that though it was warmer during the Eemian than the Holocene, the sea-ice was quite similar during the early Eemian and the early Holocene. However, after 3000 years (124 ka and 8 ka), the Eemian sea-ice volume in the Arctic was significantly larger in the Northern Hemisphere than in the Holocene.

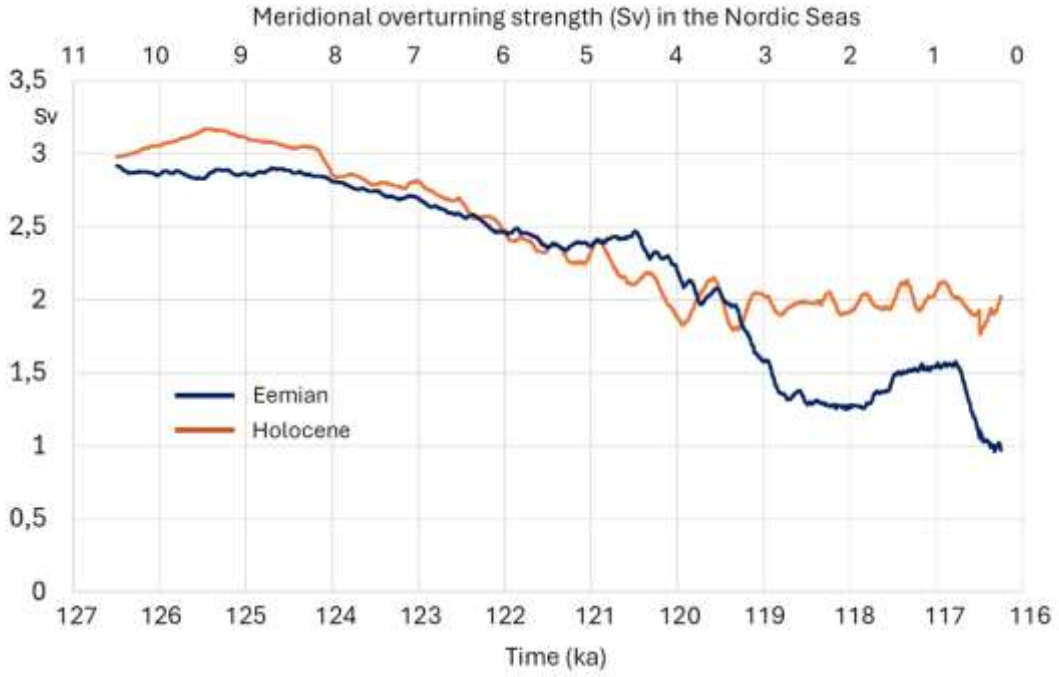

Figure 6. Evolution of the annual maximum meridional overturning streamfunction (Sv) in the Nordic Seas for the Holocene (Orange colour) and the Eemian (Blue colour). The trend shows a 1000 yr running mean.

3.4. Comparison of the Climate Simulations With Proxy-Based Reconstructions

As discussed previously for the Holocene (Arthur et al., 2023), our downscaled simulation EEM_Down depicts climate at a regional scale that is more in line with the spatial scale of proxy data than our EEM_Standard experiment. The improvement resulting from the downscaling technique will affect our results when compared to other climate model simulations and proxy-based reconstructions, particularly as the latter is impacted by local conditions. We have compared our EEM_Down and EEM_Standard results of temperature and precipitation in Europe with proxy-based reconstructions that are currently available and other climate model results to evaluate the performance of our downscaling technique.

Regarding the magnitude of change, our EEM_Down simulation agrees with the (+3 and +4 °C) anomalies reconstructed by the proxies of Capron et al. (2017) across Europe at 127 ka. Again, our EEM_Down more accurately reproduces the magnitude of precipitation anomalies; both our simulated EEM_Down and proxy-based anomalies by Capron et al. (2017) show annual precipitation between 200–400 mm/yr compared to pre-industrial, which is in close agreement. Moreover, for western Europe, our EEM_Down experiment captures the warming reconstructed by Turney and Jones (2010). The reconstruction of Turney and Jones (2010) indicates a temperature anomaly between +1 and +2 °C relative to pre-industrial which is similar to our EEM_Down simulation in western Europe. A recent reconstruction by Honiat et al. (2023) based on speleothems reported a temperature change across the southeastern Alps (46°30 ° N, 14°23 ° E) with peak temperatures at ~ 127 ka of 2.4 ± 2.8 ◦C above today's mean (1973–2002). Their reconstruction indicates that temperatures slightly decreased during the mid-Eemian (124 to 121 ka) and gradually dropped below modern-day temperatures after about 118 ka. Our simulation aligns with this study, with temperature anomalies

 doi:10.20944/preprints202502.0262.v1

up to +2 °C in the southeastern Alps. Moreover, our model simulates a stable temperature at 124 ka in this region with a slight decrease at 120 ka leading to negative temperature anomalies up to -0.5 °C which is comparable to the temperature decrease reconstructed by their study.

The output of our downscaled precipitation results in the Eemian is further compared with a comprehensive proxy-based reconstruction compiled by Scussolini et al. (2019). Their reconstruction is based on pollen, speleothems, multi-proxies and other data (LIGA members, 1991; Klotz et al., 2003; Sirocko et al., 2005; Drysdale et al., 2005; Allen and Huntley, 2009; Milner et al., 2012; Tzedakis et al., 2018). (Figure 7). The reconstruction reveals that southern and eastern Europe were wetter than pre-industrial, while Central Europe was also wetter with precipitation anomalies above +200 mm/yr (Scussolini et al., 2019). This is in line with our EEM_Down results (Figure 7), with our magnitude of precipitation anomalies between +150 to +300 mm/yr relative to preindustrial in central to eastern Europe. Lower precipitation was reconstructed in Scandinavia which is generally comparable to our EEM_Down simulation. However, our model simulates higher precipitation in the northern part of Scandinavia, which is not seen in the proxies. The proxy-based reconstructions also show that regions such as Italy and France were wetter and warmer than pre-industrial, while several locations in the northern Alps region show that average precipitation is rather similar to that of the present (Scussolini et al., 2019). The EEM_Down simulation suggests drier conditions in France and disagrees with the reconstructions here, but the model results agree with the sign of change in Southern Italy. For example, EEM_Down simulates drier conditions in France and Northern Italy by reductions of up to -100 mm/yr compared to the preindustrial and most of the northern Alps were also drier. However, our EEM_Down experiment agrees with the high precipitation reconstructed by the proxies in the southeastern part of the domain (Greece, Turkey and the Middle East) (Figure 7).

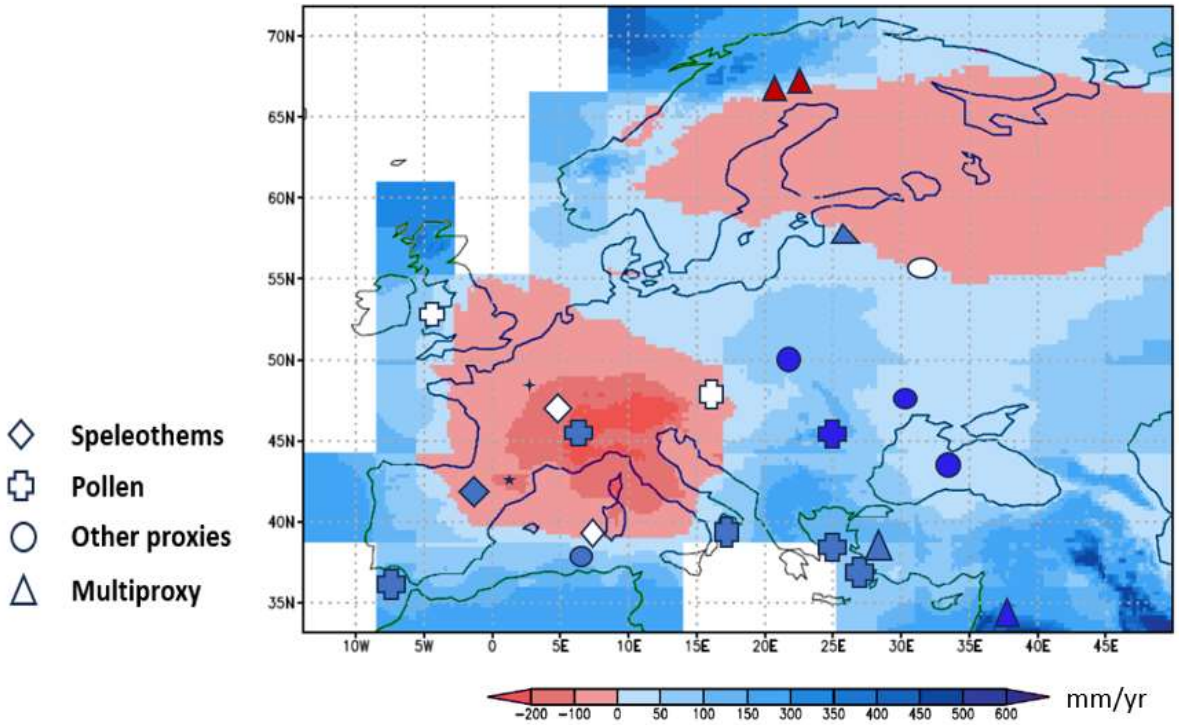

Figure 7. Annual precipitation anomalies at 127 ka relative to Pre-industrial from the EEM_Down (in colors with contours) and proxies (filled markers). Blue colors represent higher precipitation during the EEM_127 ka from climate simulations or proxies and red colors represent lower precipitation. Proxy anomalies: dark blue (much wetter Eemian), light blue (wetter), white (no discernible anomaly), light red (drier), and dark red (much drier). Different markers represent different types of proxy records (proxy data from Scussolini et al., 2019).

 doi:10.20944/preprints202502.0262.v1

Proxy-based reconstructions of Brewer et al. (2008) compared the climate evolution during the Eemian, using pollen data from 17 sites across Europe. According to their findings, the Eemian is divided into three typical parts: an early optimum, a slow cooling period, and then another abrupt drop in precipitation and temperatures. This sequence is restricted to the north of Europe, where temperatures remain stable for a longer time. The latitudinal temperature gradient varied significantly, with greater variations in the north than in the south, meaning that the reduction of temperature during this period was greater in the northern part of Europe than in the South. This is in close agreement with our temperature and precipitation trends in our simulations (Figure 2 & 3). The transition to the early Eemian in EEM_Down and EEM_Standard is marked by a slight decline in precipitation across Europe. This is a distinctive feature of the Eemian climate evolution reconstructed in previous studies (Brewer et al., 2008; Capron et al., 2017).

A reconstruction of temperatures in the Swiss Alps over the entire Eemian was done by Wilcox et al. (2020) based on speleothems. Their study found that temperatures were up to 4.3 °C warmer during the Eemian (at 127 ka) than in the present-day, while our EEM_Down experiment simulates temperature anomalies of up to 2 °C at 127 ka relative to pre-industrial in the Swiss Alps. The study suggests that higher-elevation areas may be more sensitive to warming as compared to lowland regions (Wilcox et al. 2020).

3.5. Comparison of the Model Results with Other Climate Model Simulations

The annual warming in northern Europe simulated during the early Eemian (127 ka) by EEM_Down agrees with the multi-model mean simulated by Lunt et al. (2013) and in good agreement with the CMIP6-PMIP4 lig127 k simulations (Otto- Bliesner et al., 2021). For many regions, the EEM_Down seems to be able to reproduce the sign of temperature change, simulated anomalies indicate increases in temperature, particularly throughout northern Europe. For example, this agrees with Williams et al. (2020), who simulate a high temperature anomaly in northern Europe with the HadGEM3-GC3 model done under the CMIP6/PMIP4 framework. Their model underestimates the warming reconstructed by proxies and other climate models in northern Europe with up to 1 °C temperature anomalies with respect to pre-industrial. For western Europe, our EEM_Down captures the warming simulated by the AWI-ESM model studied by Shi et al. (2022).

5. Conclusions

In this study, we have performed simulations of the Eemian climate using the standard version of the iLOVECLIM model and a version with an interactive physical downscaling applied (by increasing its horizontal atmospheric resolution from 5.56° to 0.25° latitude-longitude). We have performed transient simulations with both versions of the model and analyzed the results relative to pre-industrial. The following scientific questions have been answered.

1. *What are the magnitudes and spatial patterns of temperature and precipitation changes over Europe during the Eemian period?*

Our simulations suggest that the magnitude of temperature and precipitation varied across different regions of Europe, with some areas experiencing more pronounced warming and precipitation differences than others. The latitudinal pattern in our simulation during the Eemian shows that the warming was stronger at high latitudes than at mid-latitudes in Europe. For instance, the northern latitudes of Europe, including Scandinavia and the British Isles experienced greater temperature anomalies compared to the southern regions in both simulations. EEM_Down simulates annual temperature anomalies between +3 and +4 °C relative to pre-industrial in the northern-most part (above 65 °N) at 127 ka, while EEM_Standard simulates up to +2 °C in the same region relative to pre-industrial. Most parts of central Europe were also relatively warmer in the downscaling simulations (+0.5 to +2 °C). The late Eemian shows that annual mean temperature anomalies were almost close to 0 °C for all simulations. The simulated precipitation in the downscaling shows more

 doi:10.20944/preprints202502.0262.v1

detail information in the topographic regions and wetter conditions in the early Eemian as compared to pre-industrial. For instance, in the Scandes mountains, our EEM_Down experiment simulates wetter conditions than pre-industrial with annual mean precipitation anomalies between +150 to +300 mm/yr and shows higher spatial variability, while EEM_Standard simulates precipitation anomalies of up to +120 mm/yr relative to the pre-industrial.

2. *How do the simulated changes in temperature and precipitation compare to proxy data from the Eemian period? Is the downscaling performing better than the low-resolution model?*

Our study indicates that the EEM_Down simulation is generally in line with proxy-based reconstructions and other climate models, especially in high-elevated regions. The downscaling technique provides detailed information in mountainous regions (the Alps, and the Scandes mountains), and it simulates higher precipitation than the EEM_Standard. After comparing proxy-based reconstructions with our EEM_Down and EEM_Standard simulations, it was evident that EEM_Down more accurately represents the extent of warming in the northern region of Europe, the Alps, the western regions, and other areas reconstructed using multiple proxies. There is a good agreement for the general trend and spatial pattern in the downscaling, Our EEM_Down experiment captures the distinct patterns of change (for example, wetter conditions reconstructed by proxies in southern and eastern Europe). Compared to the pre-industrial era, most of Europe's simulated temperatures and precipitation were generally higher during the early Eemian than later during this interglacial.

3. *How different are the evolutions of the climate in the Holocene and the Eemian in Europe?*

A comparative analysis of the climate evolution in the Holocene and the Eemian in Europe reveals several key differences. While both periods experienced warmer temperatures relative to pre-industrial, the Eemian was characterized by more pronounced warmth than the Holocene. This may be expected based on the higher orbitally-forced summer insolation during most of the Eemian relative to the Holocene. The precipitation trend in the early Eemian was wetter relative to pre-industrial than the Holocene in line with the temperature trends, but the Holocene became wetter than the Eemian relative to pre-industrial during the HTM. This is because the Atlantic meridional overturning circulation (AMOC) was slightly stronger during the Holocene than the Eemian, which led to enhanced deep-water formation and reduced sea-ice cover in the Nordic Seas. Further research is needed to understand the transient evolution of precipitation during the Eemian and the Holocene climate in Europe. Current studies are more focused on snapshot experiments and only temperature within this interglacial period.

Author Contributions: FA, DMR and HR designed the study. FA, AZ, and HL performed the simulations. FA and HR wrote the manuscript with contributions from DMR, AZ and HL. All authors analyzed and interpreted the model results.

Funding: The research is financed through the European Union's Horizon 2020 research and innovation programme within the TERRANOVA project, no. 813904. The paper only reflects the views of the authors, and the European Union cannot be held responsible for any use which may be made of the information contained therein.

Data Availability Statement: The iLOVECLIM source code is accessible at http://www.elic.ucl.ac.be/modx/elic/index.php?id=289 (UCL, 2021). The developments on the iLOVECLIM source code are hosted at http://forge.ipsl.jussieu.fr/ludus (IPSL, 2021); due to copyright restrictions, they cannot be publicly accessed. Access request can be made by contacting Didier M. Roche (didier.roche@lsce.ipsl.fr). For this study, we used the model at revision 1147.

Acknowledgements: We would like to thank Prof. Gustav Strandberg from the Swedish Meteorological and Hydrological Institute and Prof Johann Jungclaus from the Max Planck Institute for Meteorology for their thorough review of the manuscript before its submission.

 doi:10.20944/preprints202502.0262.v1

Conflicts of Interest: The contact author has declared that none of the authors has any competing interests.".

Abbreviations

The following abbreviations are used in this manuscript:

GCM	General Circulation Models
PMIP	Paleoclimate Modelling Intercomparison project

References

Allen, J. R., & Huntley, B. (2009). Last Interglacial palaeovegetation, palaeoenvironments and chronology: a new record from Lago Grande di Monticchio, southern Italy. *Quaternary Science Reviews*, *28*(15–16), 1521–1538. https://doi.org/10.1016/j.quascirev.2009.02.013.

Arthur, F., Hatlestad, K., Lindholm, K.-J., Loftsgarden, K., Löwenborg, D., Solheim, S., Roche, D. M., & Renssen, H. (2024). The impact of volcanism on Scandinavian climate and human societies during the Holocene: Insights into the Fimbulwinter eruptions (536/540 AD). The Holocene, 34(5), 619-633. https://doi.org/10.1177/09596836231225718

Arthur, F., Roche, D. M., Fyfe, R., Quiquet, A., & Renssen, H. (2023). Simulations of the Holocene climate in Europe using an interactive downscaling within the iLOVECLIM model (version 1.1). *Climate of the Past*, *19*(1), 87–106. https://doi.org/10.5194/cp-19-87-2023.

Bakker, P., Masson-Delmotte, V., Martrat, B., Charbit, S., Renssen, H., Gröger, M., Krebs-Kanzow, U., Lohmann, G., Lunt, D., Pfeiffer, M., Phipps, S., Prange, M., Ritz, S., Schulz, M., Stenni, B., Stone, E., & Varma, V. (2014). Temperature trends during the Present and Last Interglacial periods – a multi-model-data comparison. *Quaternary Science Reviews*, *99*, 224–243. https://doi.org/10.1016/j.quascirev.2014.06.031.

Bereiter, B., Eggleston, S., Schmitt, J., Nehrbass-Ahles, C., Stocker, T. F., Fischer, H., Kipfstuhl, S., & Chappellaz, J. (2015). Revision of the EPICA Dome C CO2 record from 800 to 600 kyr before present. *Geophysical Research Letters*, *42*(2), 542–549. https://doi.org/10.1002/2014gl061957.

Berger, A. (1978). Long-Term Variations of Daily Insolation and Quaternary Climatic Changes. *Journal of the Atmospheric Sciences*, *35*(12), 2362–2367. https://doi.org/10.1175/1520-0469(1978)035%3C2362:LTVODI%3E2.0.CO;2.

Braconnot, P., Harrison, S. P., Kageyama, M., Bartlein, P. J., Masson-Delmotte, V., Abe-Ouchi, A., Otto-Bliesner, B., & Zhao, Y. (2012). Evaluation of climate models using palaeoclimatic data. *Nature Climate Change*, *2*(6), 417–424. https://doi.org/10.1038/nclimate1456.

Brewer, S., Guiot, J., Sánchez-Goñi, M., & Klotz, S. (2008). The climate in Europe during the Eemian: a multi-method approach using pollen data. *Quaternary Science Reviews*, *27*(25–26), 2303–2315. https://doi.org/10.1016/j.quascirev.2008.08.029.

Brovkin, V., Ganopolski, A., & Svirezhev, Y. (1997). A continuous climate-vegetation classification for use in climate-biosphere studies. *Ecological Modelling*, *101*(2–3), 251–261. https://doi.org/10.1016/s0304-3800(97)00049-5.

CAPE-members, Anderson, P., Bennike, O., Bigelow, N., Brigham-Grette, J., Duvall, M., Edwards, M., Fr'echette, B., Funder, S., Johnsen, S., Knies, J., Koerner, R., Lozhkin, A., MacDonald, G., Marshall, S., Matthiessen, J., Miller, G., Montoya, M., Muhs, D., Otto-Bliesner, B., Overpeck, J., Reeh, N., Sejrup, H.P., Turner, C., & Velichko, A. (2006).. Last Interglacial Arctic warmth confirms polar amplification of climate change. Quaternary Science Reviews, 25, 1383e1400. https://doi.org/ 10.1016/j.quascirev.2006.01.033

Capron, E., Govin, A., Feng, R., Otto-Bliesner, B., & Wolff, E. (2017). Critical evaluation of climate syntheses to benchmark CMIP6/PMIP4 127 ka Last Interglacial simulations in the high-latitude regions. *Quaternary Science Reviews*, *168*, 137–150. https://doi.org/10.1016/j.quascirev.2017.04.019.

Cheddadi, R., Mamakowa, K., Guiot, J., de Beaulieu, J. L., Reille, M., Andrieu, V., Granoszewski, W., & Peyron, O. (1998). Was the climate of the Eemian stable? A quantitative climate reconstruction from seven European pollen records. Palaeogeography, Palaeoclimatology, Palaeoecology, 143(1–3), 73–85. https://doi.org/10.1016/s0031-0182(98)00067-4.

Drysdale, R. N., Zanchetta, G., Hellstrom, J. C., Fallick, A. E., & Zhao, J. (2005). Stalagmite evidence for the onset of the Last Interglacial in southern Europe at 129 ± 1 ka. Geophysical Research Letters, 32(24). https://doi.org/10.1029/2005gl024658.

Dutton, A., & Lambeck, K. (2012). Ice Volume and Sea Level During the Last Interglacial. *Science*, *337*(6091), 216–219. https://doi.org/10.1126/science.1205749

Dyer, B., Austermann, J., D'Andrea, W. J., Creel, R. C., Sandstrom, M. R., Cashman, M., Rovere, A., & Raymo, M. E. (2021). Sea-level trends across The Bahamas constrain peak last interglacial ice melt. *Proceedings of the National Academy of Sciences*, *118*(33). https://doi.org/10.1073/pnas.2026839118.

Fischer, N., & Jungclaus, J. H. (2010). Effects of orbital forcing on atmosphere and ocean heat transports in Holocene and Eemian climate simulations with a comprehensive Earth system model. *Climate of the Past*, *6*(2), 155–168. https://doi.org/10.5194/cp-6-155-2010.

Goelzer, H., Huybrechts, P., Loutre, M. F., & Fichefet, T. (2016). Last Interglacial climate and sea-level evolution from a coupled ice sheet–climate model. *Climate of the Past*, *12*(12), 2195–2213. https://doi.org/10.5194/cp-12-2195-2016.

Goosse, H., & Fichefet, T. (1999). Importance of ice-ocean interactions for the global ocean circulation: A model study. *Journal of Geophysical Research: Oceans*, *104*(C10), 23337–23355. https://doi.org/10.1029/1999jc900215.

Goosse, H., Brovkin, V., Fichefet, T., Haarsma, R., Huybrechts, P., Jongma, J., Mouchet, A., Selten, F., Barriat, P.-Y., Campin, J.- M., Deleersnijder, E., Driesschaert, E., Goelzer, H., Janssens, I., Loutre, M.-F., Morales Maqueda, M. A., Opsteegh, T., Mathieu, P.-P., Munhoven, G., Pettersson, E. J., Renssen, H., Roche, D. M., Schaeffer, M., Tartinville, B., Timmermann, A., & Weber, S. L. (2010). Description of the Earth system model of intermediate complexity LOVECLIM version 1.2, *Geoscientific Model Development*, 3, 603–633. https://doi.org/10.5194/gmd-3-603-2010.

Honiat, C., Koltai, G., Dublyansky, Y., Edwards, R. L., Zhang, H., Cheng, H., & Spötl, C. (2023). A paleoprecipitation and paleotemperature reconstruction of the Last Interglacial in the southeastern Alps. *Climate of the Past*, *19*(6), 1177–1199. https://doi.org/10.5194/cp-19-1177-2023..

Klotz, S., Guiot, J., & Mosbrugger, V. (2003). Continental European Eemian and early Würmian climate evolution: comparing signals using different quantitative reconstruction approaches based on pollen. *Global and Planetary Change*, *36*(4), 277–294. https://doi.org/10.1016/s0921-8181(02)00222-9.

Klotz, S., Müller, U., Mosbrugger, V., de Beaulieu, J. L., & Reille, M. (2004). Eemian to early Würmian climate dynamics: history and pattern of changes in Central Europe. *Palaeogeography, Palaeoclimatology, Palaeoecology*, *211*(1–2), 107–126. https://doi.org/10.1016/j.palaeo.2004.04.009.

Lhardy, F., Bouttes, N., Roche, D. M., Abe-Ouchi, A., Chase, Z., Crichton, K. A., Ilyina, T., Ivanovic, R., Jochum, M., Kageyama, M., Kobayashi, H., Liu, B., Menviel, L., Muglia, J., Nuterman, R., Oka, A., Vettoretti, G., & Yamamoto, A. (2021). A First Intercomparison of the Simulated LGM Carbon Results Within PMIP-Carbon: Role of the Ocean Boundary Conditions. Paleoceanography and Paleoclimatology, 36(10). https://doi.org/10.1029/2021pa004302

Li, H., Renssen, H., & Roche, D. M. (2019). Global vegetation distribution driving factors in two Dynamic Global Vegetation Models of contrasting complexities. *Global and Planetary Change*, *180*, 51–65. https://doi.org/10.1016/j.gloplacha.2019.05.009.

Li, H., Renssen, H., & Roche, D. M. (2020). Modeling climate-vegetation interactions during the last interglacial: The impact of biogeophysical feedbacks in North Africa. ***Quaternary Science Reviews,*** 249. doi: 10.1016/j.quascirev.2020.106609.

LIGA members, (1991). The last interglacial in high latitudes of the Northern Hemisphere: Terrestrial and marine evidence. *Quaternary International*, 10–12, 9–28. https://doi.org/10.1016/1040-6182(91)90038- P.

Lunt, D. J., Abe-Ouchi, A., Bakker, P., Berger, A., Braconnot, P., Charbit, S., Fischer, N., Herold, N., Jungclaus, J. H., Khon, V. C., Krebs-Kanzow, U., Langebroek, P. M., Lohmann, G., Nisancioglu, K. H., Otto-Bliesner, B. L., Park, W., Pfeiffer, M., Phipps, S. J., Prange, M., Rachmayani, R., Renssen, H., Rosenbloom, N., Schneider, B., Stone, E. J., Takahashi, K., Wei, W., Yin, Q., & Zhang, Z. S. (2013). A multi-model assessment of last interglacial temperatures, *Climate of the past*, 9, 699–717. https://doi.org/10.5194/cp-9-699-2013.

McKay, N. P., Overpeck, J. T., & Otto-Bliesner, B. L. (2011). The role of ocean thermal expansion in Last Interglacial Sea level rise. *Geophysical Research Letters*, *38*(14). https://doi.org/10.1029/2011gl048280.

Milner, A. M., Collier, R. E., Roucoux, K. H., Müller, U. C., Pross, J., Kalaitzidis, S., Christanis, K., & Tzedakis, P. C. (2012). Enhanced seasonality of precipitation in the Mediterranean during the early part of the Last Interglacial. *Geology*, *40*(10), 919–922. https://doi.org/10.1130/g33204.1.

NEEM community members, (2013). Eemian interglacial reconstructed from a Greenland folded ice core. *Nature,* 493, 489–494. https://doi.org/10.1038/nature11789.

Opsteegh, J. D., Haarsma, R. J., Selten, F. M., & Kattenberg, A. (1998). ECBILT: a dynamic alternative to mixed boundary conditions in ocean models, *Tellus A*, 50, 348–367. https://doi.org/10.1034/j.1600-0870.1998.t01-1-00007.x.

Otto-Bliesner, B. L., Braconnot, P., Harrison, S. P., Lunt, D. J., Abe-Ouchi, A., Albani, S., Bartlein, P. J., Capron, E., Carlson, A. E., Dutton, A., Fischer, H., Goelzer, H., Govin, A., Haywood, A., Joos, F., LeGrande, A. N., Lipscomb, W. H., Lohmann, G., Mahowald, N., Nehrbass-Ahles, C., Pausata, F. S. R., Peterschmitt, J.-Y., Phipps, S. J., Renssen, H., & Zhang, Q. (2017). The PMIP4 contribution to CMIP6 – Part 2: Two interglacials, scientific objective and experimental design for Holocene and Last Interglacial simulations. *Geoscientific Model Development*, 10, 3979–4003. https://doi.org/10.5194/gmd-10-3979-2017.

Otto-Bliesner, B. L., Brady, E. C., Zhao, A., Brierley, C. M., Axford, Y., Capron, E., Govin, A., Hoffman, J. S., Isaacs, E., Kageyama, M., Scussolini, P., Tzedakis, P. C., Williams, C. J. R., Wolff, E., Abe-Ouchi, A., Braconnot, P., Ramos Buarque, S., Cao, J., de Vernal, A., Guarino, M. V., Guo, C., LeGrande, A. N., Lohmann, G., Meissner, K. J., Menviel, L., Morozova, P. A., Nisancioglu, K. H., O'ishi, R., Salas y Mélia, D., Shi, X., Sicard, M., Sime, L., Stepanek, C., Tomas, R., Volodin, E., Yeung, N. K. H., Zhang, Q., Zhang, Z., & Zheng, W. (2021). Large-scale features of Last Interglacial climate: results from evaluating the *lig127k* simulations for the Coupled Model Intercomparison Project (CMIP6)–Paleoclimate Modeling Intercomparison Project (PMIP4). *Climate of the. Past*, 17, 63–94. https://doi.org/10.5194/cp-17-63-2021.

Otto-Bliesner, B. L., Park,W., Pfeiffer, M., Phipps, S. J., Prange, M., Rachmayani, R., Renssen, H., Rosenbloom, N., Schneider, B., Stone, E. J., Takahashi, K., Wei, W., Yin, Q., & Zhang, Z. S. (2013). A multi-model assessment of last interglacial temperatures. *Climate of the Past*, 9, 699–717. https://doi.org/10.5194/cp-9- 699-2013.

Pedersen, R. A., Langen, P. L., & Vinther, B. M. (2016). The last interglacial climate: comparing direct and indirect impacts of insolation changes. *Climate Dynamics*, *48*(9–10), 3391–3407. https://doi.org/10.1007/s00382-016-3274-5.

Quiquet, A., Dumas, C., Paillard, D., Ramstein, G., Ritz, C., & Roche, D. M. (2021). Deglacial Ice Sheet Instabilities Induced by Proglacial Lakes. *Geophysical Research Letters*, *48*(9). https://doi.org/10.1029/2020gl092141.

Quiquet, A., Roche, D. M., Dumas, C., & Paillard, D. (2018). Online dynamical downscaling of temperature and precipitation within the LOVECLIM model (version 1.1). *Geoscientific Model Development*, *11*(1), 453–466. https://doi.org/10.5194/gmd-11-453-2018.

Renssen, H., Goosse, H., Fichefet, T., Brovkin, V., Driesschaert, E., & Wolk, F. (2004). Simulating the Holocene climate evolution at northern high latitudes using a coupled atmosphere-sea ice-ocean-vegetation model. *Climate Dynamics*, *24*(1), 23–43. https://doi.org/10.1007/s00382-004-0485-y

Renssen, H., Seppä, H., Heiri, O., Roche, D. M., Goosse, H., & Fichefet, T. (2009). The spatial and temporal complexity of the Holocene thermal maximum. *Nature Geoscience*, *2*(6), 411–414. https://doi.org/10.1038/ngeo513

Roche, D. M., Dumas, C., Bügelmayer, M., Charbit, S., & Ritz, C. (2014). Adding a dynamical cryosphere to iLOVECLIM (version 1.0): coupling with the GRISLI ice-sheet model. *Geoscientific Model Development*, 7, 1377–1394. https://doi.org/10.5194/gmd-7-1377-2014.

Schilt, A., Baumgartner, M., Blunier, T., Schwander, J., Spahni, R., Fischer, H., & Stocker, T. F. (2010). Glacial–interglacial and millennial-scale variations in the atmospheric nitrous oxide concentration during the last 800,000 years. *Quaternary Science Reviews*. *29*(1–2), 182–192. https://doi.org/10.1016/j.quascirev.2009.03.011.

Scussolini, P., Bakker, P., Guo, C., Stepanek, C., Zhang, Q., Braconnot, P., Cao, J., Guarino, M. V., Coumou, D., Prange, M., Ward, P. J., Renssen, H., Kageyama, M., Otto-Bliesner, B., & Aerts, J. C. J. H. (2019). Agreement between reconstructed and modeled boreal precipitation of the Last Interglacial. *Science advances*, *5*(11), eaax7047. https://doi.org/10.1126/sciadv.aax7047.

Shi, X., Werner, M., Wang, Q., Yang, H., & Lohmann, G. (2022). Simulated Mid-Holocene and Last Interglacial Climate Using Two Generations of AWI-ESM. *Journal of Climate*, *35*(23), 7811–7831. https://doi.org/10.1175/jcli-d-22-0354.1.

Sirocko, F., Seelos, K., Schaber, K., Rein, B., Dreher, F., Diehl, M., Lehne, R., Jäger, K., Krbetschek, M., & Degering, D. (2005). A late Eemian aridity pulse in central Europe during the last glacial inception. *Nature*, *436*(7052), 833–836. https://doi.org/10.1038/nature03905.

Turney, C. S., & Jones, R. T. (2010). Does the Agulhas Current amplify global temperatures during super-interglacials? *Journal of Quaternary Science*, *25*(6), 839–843. https://doi.org/10.1002/jqs.1423.

Tzedakis, P. C., Drysdale, R. N., Margari, V., Skinner, L. C., Menviel, L., Rhodes, R. H., Taschetto, A. S., Hodell, D. A., Crowhurst, S. J., Hellstrom, J. C., Fallick, A. E., Grimalt, J. O., McManus, J. F., Martrat, B., Mokeddem, Z., Parrenin, F., Regattieri, E., Roe, K., & Zanchetta, G. (2018). Enhanced climate instability in the North Atlantic and southern Europe during the Last Interglacial. *Nature Communications*, *9*(1). https://doi.org/10.1038/s41467-018-06683-3.

Wilcox, P. S., Honiat, C., Trüssel, M., Edwards, R. L., & Spötl, C. (2020). Exceptional warmth and climate instability occurred in the European Alps during the Last Interglacial period. *Communications Earth & Environment*, *1*(1). https://doi.org/10.1038/s43247-020-00063-w

Williams, C. J. R., Guarino, M. V., Capron, E., Malmierca-Vallet, I., Singarayer, J. S., Sime, L. C., Lunt, D. J., & Valdes, P. J. (2020). CMIP6/PMIP4 simulations of the mid-Holocene and Last Interglacial using HadGEM3: comparison to the pre-industrial era, previous model versions and proxy data. *Climate of the Past*, 16(4), 1429–1450. https://doi.org/10.5194/cp-16-1429-2020.

Zhang, Y., Renssen, H., & Seppä, H. (2016). Effects of melting ice sheets and orbital forcing on the early Holocene warming in the extratropical Northern Hemisphere. *Climate of the Past*, *12*(5), 1119–1135. https://doi.org/10.5194/cp-12-1119-2016.